Dual-polarized all-angle cloaking of a dielectric nanowire by helical graphene ribbons

Vitalii I. Shcherbinin,[1,2] Yuliya K. Moskvitina,[2] Volodymyr I. Fesenko,[1,3,*] and Vladimir R. Tuz[1,3,†]

[1]*International Center of Future Science, State Key Laboratory of Integrated Optoelectronics, College of Electronic Science and Engineering, Jilin University, 2699 Qianjin Street, Changchun 130012, China*

[2]*National Science Center "Kharkiv Institute of Physics and Technology," National Academy of Sciences of Ukraine, 1, Akademicheskaya Street, Kharkiv 61108, Ukraine*

[3]*Institute of Radio Astronomy, National Academy of Sciences of Ukraine, 4 Mystetstv Street, Kharkiv 61002, Ukraine*

(Received 18 April 2019; published 22 July 2019)

Scattering from a dielectric nanowire coated by helical graphene strips (nanoribbons) is investigated for a dual-polarized wave at oblique incidence. In the long-wavelength approximation, the helical strips are treated as a homogeneous layer with averaged tensor conductivity. It is shown that the performance of well-known surface cloaks in the form of graphene monolayer, axial, and azimuthal graphene strips can be deteriorated in a wide range of incidence angles. To overcome this problem, helical graphene strips are proposed as an advanced metasurface for dual-polarized all-angle cloaking of the dielectric nanowire in the terahertz band. It is found that such metasurface suppresses scattering from the nanowire more efficiently as compared to graphene monolayer, regardless of the angle of wave incidence. Moreover, dual-polarized all-angle cloaking of the dielectric nanowire can be broadly tuned in frequency with parameters of helical graphene strips.

DOI: 10.1103/PhysRevB.100.035428

I. INTRODUCTION

Electromagnetic cloaking of objects, which makes them less visible to an observer, is a subject of much interest for decades [1]. At present, there are a number of well-established cloaking methods, ranging from transformation-based cloaking [2–5] for microwaves to a plasmonic one [6–10] at infrared and visible frequencies. Our interest is in mantle cloaking of dielectric objects by conducting surfaces [11,12]. Such a method relies on scattering cancellation due to destructive interference between fields scattered from the object and the cloak [6]. One of its advantages is the thinness of the cloak, which, in contrast to transformation-based and plasmonic counterparts, can be conformal to the object. Another advantage is that the mantle cloak does not isolate the object electromagnetically from ambient space. Together, these beneficial properties make mantle cloaking particularly suitable for use in novel sensor and antenna applications [13,14]. In these applications, objects to be cloaked usually have a cylindrical form.

In the terahertz frequency band, graphene is known to have a number of unique properties to serve as a thinnest possible mantle cloak [15]. First, graphene is a good conducting material at the terahertz frequencies. Second, its intrinsic losses are low enough to make the cloaking performance of the graphene monolayer close to that of an ideal cloak. Third, graphene conductivity can be tuned by applied bias voltage, thereby providing the possibility for dynamical tuning of cloaking frequency. All these properties ensure efficient scattering suppression for single and multiple dielectric cylinders with uniform graphene coating [15–18]. Cloaking performance can be further improved using a periodic array of subwavelength graphene nanopatches [19], which act as a metasurface with averaged conductivity. Such a cloak demonstrates good performance for both dielectric and metallic cylindrical objects, as well as for elliptical structures [20] and conducting wedges [21]. Along with graphene nanopatches, other subwavelength elements find use in the design of graphene-based metasurfaces. An example is a metasurface composed of periodic graphene nanodisks [22], which makes it possible to enhance the frequency bandwidth of a cylindrical mantle cloak. It should be emphasized that good cloaking performance of graphene monolayer and graphene-based metasurfaces is demonstrated in [15–22] for objects illuminated by normally incident waves of single (TE or TM) polarization.

Ideally, mantle cloak should maximally reduce wave scattering from a given object in a broad frequency band, as well as be insensitive to polarization of incident wave and angle of incidence. As emphasized in Ref. [23], the design of such an advanced cloak is a challenging task, mainly because of the cross-polarization coupling. Therefore, to the best of our knowledge, the mantle cloak capable of meeting all the above-mentioned requirements is not yet available. For dielectric and metallic objects in the microwave frequency band, an anisotropic metasurface cloak, which can minimize scattering of both TE- and TM-polarized incident waves with the same frequencies, is investigated in [24]. The metasurface of interest is in the form of an array of orthogonal metallic strips. In the case of dielectric objects, its cloaking principle relies on the selective ability of conducting strips to suppress scattering of electromagnetic waves having an electric field parallel to the direction of strips [25]. Thus, the widths of axial and azimuthal strips around a dielectric cylinder can be varied to manipulate scattering of waves with orthogonal TM and

*volodymyr.i.fesenko@gmail.com
†tvr@jlu.edu.cn; tvr@rian.kharkov.ua

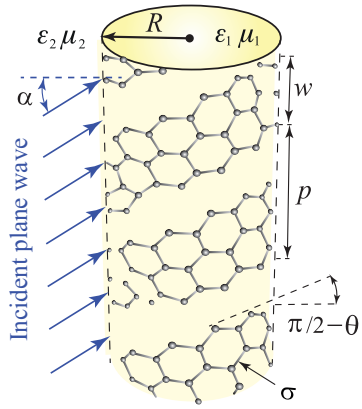

FIG. 1. Dielectric cylinder coated by helical graphene strips for oblique wave incidence.

TE polarizations independently and, if necessary, to achieve simultaneous suppression of their scattering at the desired cloaking frequency. In Ref. [24], a metasurface composed of metallic strips was designed to suppress scattering of both TM- and TE-polarized waves from a given object under normal incidence. Therefore, in the case of oblique illumination, which is always associated with cross coupling of TE and TM polarizations for scattered field, the cloaking performance of this metasurface can be nonoptimal.

Hence, to achieve dual-polarized all-angle cloaking of a dielectric nanowire in the terahertz band, it is necessary to apply a new design of a graphene-based metasurface. In such a design, it is important to keep in mind that there is a fundamental trade-off between bandwidth and total scattering reduction provided by a cloak [1,26]. Therefore, our present investigation is not concerned with the requirement on frequency bandwidth, but is aimed at finding the conditions for the most efficient cancellation of wave scattering from a dielectric nanowire. As a cloaking metasurface, we consider helical graphene strips (ribbons). In the long-wavelength approximation, such strips are characterized by the averaged conductivity of tensor form [27]. At present, there are a lot of fabrication techniques of graphene nanoribbons [28]. This fact inspires the hope that one of these techniques can be useful in the fabrication of the helical graphene strips under consideration.

II. NANOWIRE COATED BY HELICAL GRAPHENE STRIPS

Consider a cylindrical wire of radius R, relative permittivity ε_1, and permeability μ_1. The wire is coated by helical graphene strips and embedded in outside ambient with relative constitutive parameters ε_2 and μ_2. Graphene strips have the pitch angle θ, the width w, and the period p (Fig. 1).

The graphene-coated wire is under oblique incidence of the plane electromagnetic wave with the frequency ω. In cylindrical coordinates $\{r, \varphi, z\}$, the incident field is considered to have the general form [29–32]

$$\begin{Bmatrix} H_z^i \\ E_z^i \end{Bmatrix} = \begin{Bmatrix} H_0 \\ E_0 \end{Bmatrix} \sum_{n=-\infty}^{\infty} i^n J_n(k_2 r) F_n, \tag{1}$$

where $H_0 = [0.5(1+Q)]^{1/2}$ and $E_0 = -iPH_0 = -i[0.5(1-Q)]^{1/2}\exp(i\beta)$ are (up to a constant) the amplitudes of electric field components of incident wave in two orthogonal directions perpendicular to the wave incidence (see Refs. [31,32] for more details), $Q \in [-1, 1]$, $\beta \in [-\pi, \pi]$, $k_2^2 = \varepsilon_2\mu_2 k^2 - k_z^2$, $k = \omega/c$, $k_z = k\sin\alpha$, α is the incidence angle with respect to the $\{r, \varphi\}$ plane, $J_n(\cdot)$ is the Bessel function of nth order, $F_n = \exp(-i\omega t + ik_z z + in\varphi)$. For $E_0 = 0$ ($Q = 1$, $P = 0$) and $H_0 = 0$ ($Q = -1$, $P = \infty$) the illuminating wave has TE and TM polarizations, respectively, while for $Q = 0$ ($|P| = 1$) the wave is dual polarized. Dual-polarized incident waves with $P = \pm i$ and $P = \pm 1$ have linear and circular polarizations, respectively.

The scattered field and the field inside the wire can be expanded in terms of azimuthal harmonics as

$$\begin{Bmatrix} H_z^s \\ E_z^s \end{Bmatrix} = H_0 \sum_{n=-\infty}^{\infty} \begin{Bmatrix} c_n \\ d_n \end{Bmatrix} i^n H_n^{(1)}(k_2 r) F_n, \tag{2}$$

$$\begin{Bmatrix} H_{z1} \\ E_{z1} \end{Bmatrix} = H_0 \sum_{n=-\infty}^{\infty} \begin{Bmatrix} a_n \\ b_n \end{Bmatrix} i^n J_n(k_1 r) F_n = \sum_{n=-\infty}^{\infty} \begin{Bmatrix} H_{z1}^n \\ E_{z1}^n \end{Bmatrix} F_n, \tag{3}$$

respectively. Here $k_1^2 = \varepsilon_1\mu_1 k^2 - k_z^2$, $H_n^{(1)}(\cdot)$ is the Hankel function of the first kind, and a_n, b_n, c_n, and d_n are the unknowns, which are found from the conditions imposed on the wave field at the wire surface $r = R$.

Assuming that the wavelength $\lambda = 2\pi/k$ of the incident wave far exceeds the period p of graphene strips, one can approximate the strip-loaded surface of the wire by a homogeneous surface (graphene-based metasurface). The resulting metasurface possesses tensor conductivity and is governed by the following averaged boundary conditions at $r = R$ (see Ref. [27] and Appendix A):

$$\begin{aligned} E_{z1}^n &= E_{z2}^n, \quad H_{z2}^n - H_{z1}^n = -\sigma_{\varphi\varphi} E_{\varphi 1}^n - \sigma_{\varphi z} E_{z1}^n, \\ E_{\varphi 1}^n &= E_{\varphi 2}^n, \quad H_{\varphi 2}^n - H_{\varphi 1}^n = \sigma_{zz} E_{z1}^n + \sigma_{z\varphi} E_{\varphi 1}^n, \end{aligned} \tag{4}$$

where $\sigma_{\varphi\varphi} = \sigma_\perp \cos^2\theta + \sigma_\parallel \sin^2\theta$, $\sigma_{zz} = \sigma_\parallel \cos^2\theta + \sigma_\perp \sin^2\theta$, $\sigma_{\varphi z} = \sigma_{z\varphi} = (\sigma_\parallel - \sigma_\perp)\sin\theta\cos\theta$, $\sigma_{\perp,\parallel} = (Z_{\perp,\parallel} + Z_g^{av})^{-1}$, $Z_g^{av} = u/\sigma$, $u = w/p$, $\sigma = \sigma(\omega)$ is the conductivity of graphene strips,

$$\begin{aligned} Z_\parallel &= -iqZ_0 N\mu_\alpha \ln[\sin^{-1}(0.5\pi u)], \\ Z_\perp &= iZ_0(qN\varepsilon_\alpha \ln\{\sin^{-1}[0.5\pi(1-u)]\})^{-1}, \end{aligned} \tag{5}$$

and $q = 1 - k_\parallel^2/(\varepsilon_\alpha\mu_\alpha k^2)$, $N = 2p/\lambda$, $\varepsilon_\alpha = \varepsilon_1 + \varepsilon_2$, $\mu_\alpha = \mu_1\mu_2/(\mu_1 + \mu_2)$, Z_0 is the impedance of free space, and $k_\parallel^2 = (k_z\sin\theta + nR^{-1}\cos\theta)^2$.

In Eq. (4),

$$\begin{Bmatrix} H_{z2} \\ E_{z2} \end{Bmatrix} = \begin{Bmatrix} H_z^i + H_z^s \\ E_z^i + E_z^s \end{Bmatrix} = \sum_{n=-\infty}^{\infty} \begin{Bmatrix} H_{z2}^n \\ E_{z2}^n \end{Bmatrix} F_n, \tag{6}$$

and φ components of the electromagnetic field are expressed in terms of Eqs. (1)–(3).

For axial ($\theta = 0°$) and azimuthal ($\theta = 90°$) graphene strips one has $\sigma_{z\varphi} = \sigma_{\varphi z} = 0$. In this case, assuming that the strip conductivity is high enough ($Z_g^{av} \approx 0$), one can easily reduce

Eqs. (1)–(4) to the problem of wave scattering from a dielectric cylinder with periodic vertical and circumferential metallic strips for normal ($k_z = 0$) [25] or oblique [33] incidence. For these structures reasonable accuracy of the averaged boundary conditions (4) can be shown by comparison with full-wave simulations [25,33].

Substitution of Eqs. (1)–(3) into Eq. (4) gives the system of equations for unknown amplitudes a_n, b_n, c_n, and d_n of azimuthal spatial harmonics in relation to the cross-polarization parameter P of the incident wave (see Appendix B). With the amplitudes c_n and d_n of scattered field, one obtains the scattering efficiency [29]

$$Q_{\text{sca}} = \frac{2}{kR(1+|P|^2)} \sum_{n=-\infty}^{\infty} (|c_n|^2 + |d_n|^2), \tag{7}$$

which serves as a measure of visibility for a cylindrical wire at a given wave frequency and angle of incidence. Note that in the case of a metasurface composed of helical graphene strips, the cross-polarization coupling cannot be neglected for scattered wave, even though normally incident wave is considered. This is because the metasurface conductivity has a form of tensor with nonzero off-diagonal components $\sigma_{z\varphi}$ and $\sigma_{\varphi z}$. Such a property distinguishes helical graphene strips from other metasurfaces aimed at electromagnetic cloaking of cylindrical objects.

In what follows we use the above-described theory to simulate scattering of TE-, TM-, and dual-polarized waves from a dielectric wire coated by graphene strips. In the simulations, the dual-polarized incident wave, if any, is assumed to have the following parameters: $Q = 0$, $\beta = 0$ ($P = 1$), unless otherwise stated.

III. CLOAKING WITH GRAPHENE MONOLAYER, AXIAL, AND AZIMUTHAL GRAPHENE STRIPS

As the object to be cloaked, we consider a dielectric nanowire in free space ($\varepsilon_2 = 1$, $\mu_2 = 1$). The nanowire is under oblique incidence of a dual-polarized plane wave and has the following parameters: $R = 0.5$ μm, $\varepsilon_1 = 3.9$ (SiO_2), and $\mu_1 = 1$. For normal incidence ($\alpha = 0$) of TE-polarized ($P = 0$) and TM-polarized ($P = \infty$) waves, scattering characteristics of such nanowire coated by a graphene monolayer ($u = 1$) can be found in [16–18] and are used as a benchmark for our simulations. In the following, the conductivity $\sigma(\omega)$ of graphene coating is found from the widely accepted Kubo formula [34] for the temperature of 300 K, the chemical potential of 0.5 eV, and the relaxation time 1.84×10^{-13} s [see Fig. 1(b) of Ref. [35] and Appendix C]. As discussed in Ref. [21], the Kubo formula is valid for graphene-based metasurfaces, if the frequency of incident wave satisfies the condition $\hbar\omega < 0.2$ eV, where $\hbar$ is the reduced Planck constant and $\hbar\omega = 0.2$ eV is the optical phonon threshold [36]. For this reason, we restrict our further consideration to the frequencies below 25 THz, which correspond to $\hbar\omega < 0.1$ eV.

For reference, we first investigate the visibility of a bare ($u = 0$) dielectric nanowire under oblique incidence of the dual-polarized plane wave. Figure 2 shows scattering efficiency Q_{sca} of the dielectric nanowire as a function of the wave frequency $f_r = \omega/(2\pi)$ and the incidence angle α ($\{f_r, \alpha\}$ plane). It can be seen that Q_{sca} increases with increasing frequency of the illuminating wave for any α [15,16,19,37]. Generally, the higher the incidence angle, the lower the scattering from the nanowire. The exceptional angles are those near the grazing incidence ($\alpha \approx 90°$), which is characterized by an increased contribution of the TE polarization to the scattered field due to the cross-polarization coupling.

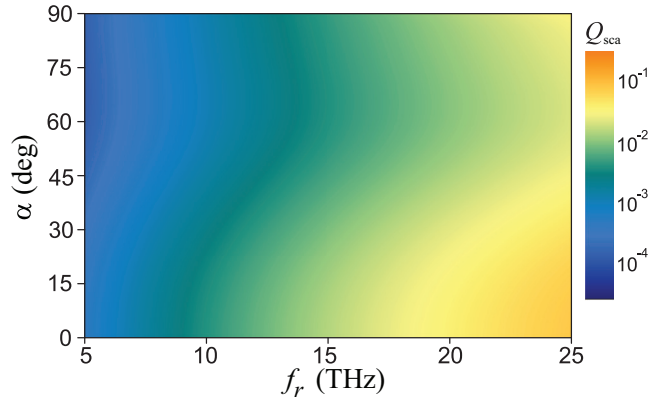

FIG. 2. Scattering efficiency Q_{sca} of a bare dielectric nanowire illuminated by a dual-polarized wave at oblique incidence.

It is well known that homogeneous graphene coating ($u = 1$) can drastically suppress the scattering from a dielectric cylinder in a certain frequency band [15,16]. For normally incident TE-, TM-, and dual-polarized waves this effect can be clearly seen from Fig. 3. Note that for the scattered field there is no cross-polarization coupling in this case. For comparison purposes, we also show data calculated by COMSOL Multiphysics in Ref. [17] for TE and TM incident waves. From Fig. 3 one can see a good agreement between these data and our simulations. Exceptions are the extrema of scattering efficiency. This is because Ref. [17] considers a graphene monolayer with low losses. Data relative to the effect of Ohmic losses (relaxation time) on wave scattering from a graphene-coated dielectric nanowire can be found in Ref. [15].

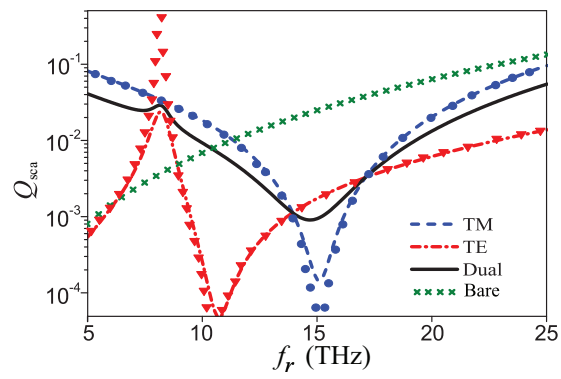

FIG. 3. Scattering efficiency versus wave frequency for a graphene-coated nanowire under normal incidence ($\alpha = 0°$) of TE-, TM-, and dual-polarized waves. Results of Ref. [17] are shown by circular and triangular markers. Scattering efficiency of a bare nanowire illuminated by a normally incident dual-polarized wave is depicted for comparison.

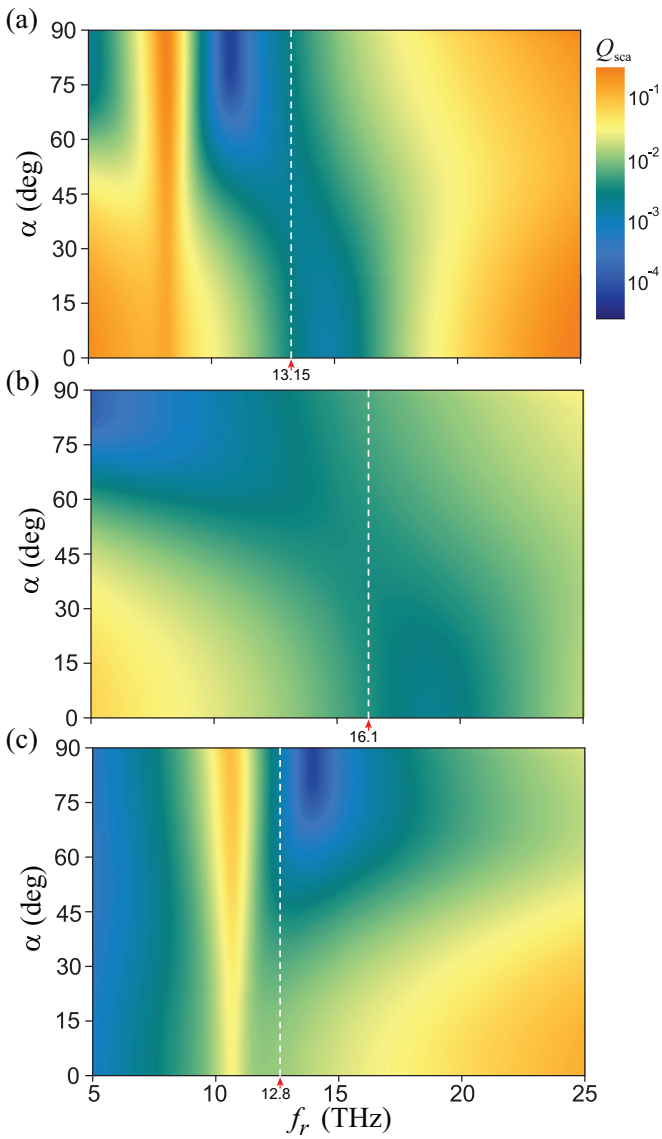

FIG. 4. Scattering efficiency Q_{sca} versus wave frequency and incidence angle for a dielectric nanowire coated by (a) graphene monolayer, (b) axial, and (c) azimuthal graphene strips at oblique incidence of a dual-polarized wave. In the cases (a), (b), and (c), the optimal frequencies of all-angle cloaking equal 13.15 THz ($Q_{sca}^{max} = 1.8 \times 10^{-3}$), 16.1 THz ($Q_{sca}^{max} = 1.3 \times 10^{-2}$), and 12.8 THz ($Q_{sca}^{max} = 2.1 \times 10^{-2}$), respectively, and are shown by the white dashed lines.

As Fig. 3 suggests, for TE- and TM-polarized incident waves the minimum scattering from the graphene-coated nanowire is attained at different frequencies [17,38]. As a consequence, when compared to these waves, for normally incident dual-polarized waves the minimum scattering efficiency is shifted in frequency and increases at least by an order of magnitude. The cloaking ability of the graphene monolayer is further deteriorated with increasing incidence angle α [Fig. 4(a)]. In this process, the minimum scattering efficiency shifts toward lower frequencies. As mentioned above, this is explained by the increase in the TE-polarized part of the scattered field [13].

As can be seen from Fig. 4(a), for any α the dielectric nanowire can be efficiently cloaked by the graphene monolayer in a certain frequency band of dual-polarized incident wave, but features enhanced scattering in other frequencies. In this regard, the most optimal frequency of all-angle cloaking is 13.15 THz, which corresponds to relatively low visibility of the wire for any incidence angle α. In this case, the maximal scattering efficiency $Q_{sca}^{max} = \max\{Q_{sca}(\alpha)\}$ is about 1.8×10^{-3} and is attained for $\alpha = 0$. In principle, the optimal frequency of all-angle cloaking can be tuned with chemical potential of graphene. Such a possibility is a matter of common knowledge [15–19] and therefore is not considered in our study.

For generality, we also investigate the ability of extensively studied axial and azimuthal strips to cloak the dielectric nanowire under oblique incidence of a dual-polarized wave. In all our subsequent simulations, the period of strips is kept constant and fulfills the requirement $N = 0.1kR$. In the case of $u = 0.6$, Figs. 4(b) and 4(c) show the scattering efficiency in the $\{f_r, \alpha\}$ plane for a dielectric nanowire coated by axial ($\theta = 0°$) and azimuthal ($\theta = 90°$) graphene strips, respectively. Compared to the graphene monolayer [see Fig. 4(a)], such strips induce much larger scattering in a wide range of frequencies, including optimal ones for all-angle cloaking. In the case of axial and azimuthal graphene strips with $u = 0.6$, these optimal frequencies equal 16.1 and 12.8 THz, respectively [see Figs. 4(b) and 4(c)]. It is evident that such a cloaking satisfies the condition $Q_{sca}^{max} > 10^{-2}$ and therefore is far from ideal.

It is seen from Figs. 4(b) and 4(c) that the axial strips provide the most efficient scattering cancellation for a normally incident wave, while azimuthal strips possess the improved ability to cloak the dielectric nanowire under grazing incidence. This is explained by two facts. First, conducting strips suppress scattering of waves, which have an electric field parallel to the strips [25]. Second, for normal incidence ($\alpha = 0°$) there is a mostly TM-polarized scattered wave with dominant axial electric field. The contribution of TE polarization to a scattered field is minor in this case (see Fig. 3). This contribution grows in importance with increasing incidence angle and attains maximum at grazing incidence ($\alpha = 90°$). From the above reasoning, it is of interest to investigate the all-angle scattering characteristics of helical graphene strips coiled around the dielectric nanowire to be cloaked.

IV. DUAL-POLARIZED ALL-ANGLE CLOAKING WITH HELICAL GRAPHENE STRIPS

First we consider a dual-polarized wave normally incident ($\alpha = 0°$) on a dielectric nanowire coated by graphene strips having the pitch angle θ and the width-to-period ratio u. For $u = 0.6$ the scattering efficiency Q_{sca} as a function of θ and frequency of illuminating wave is shown in Fig. 5(a). The minimum scattering shifts toward lower frequencies with an increase in pitch angle. What is more interesting, in the case of helical graphene strips, which always lead to cross-polarization coupling for scattered field, the minimum scattering efficiency is lower than that for both axial and azimuthal strips. For any nonzero width of graphene strips there is an absolute scattering minimum relative to a certain

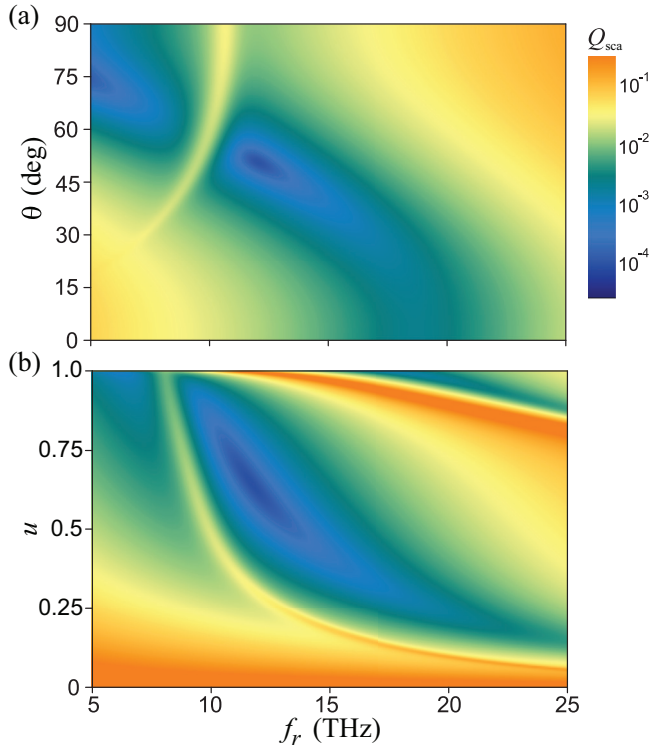

FIG. 5. Frequency-dependent scattering efficiency of a dielectric nanowire illuminated by a normally incident ($\alpha = 0°$) dual-polarized wave as a function of (a) pitch angle θ ($u = 0.6$) and (b) width-to-period ratio u ($\theta = 50°$) of helical graphene strips.

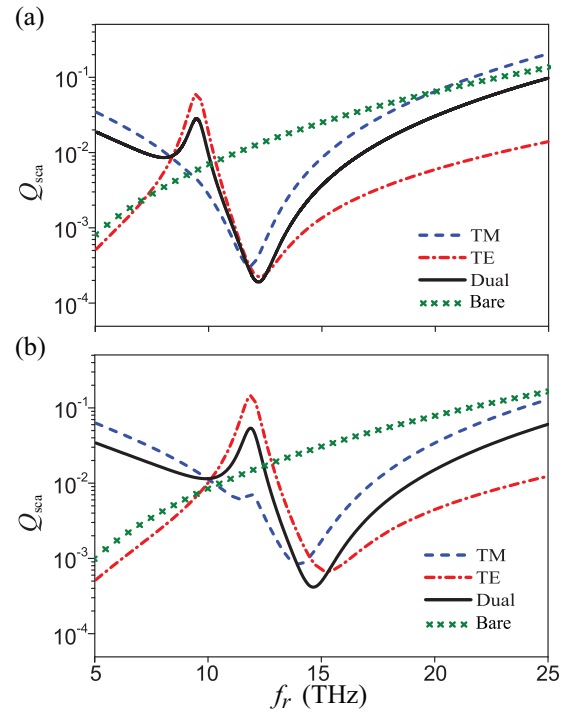

FIG. 6. The same as in Fig. 3, but for a dielectric nanowire coated by helical graphene strips with (a) $u = 0.6$, $\theta = 50°$ and (b) $u = 0.36$, $\theta = 55°$.

value of the pitch angle θ. In the case of $u = 0.6$, this value is about 50°. The formation of such minimal visibility is due to the fact that helical graphene strips, as opposed to graphene monolayer (Fig. 3), provide efficient scattering cancellation for TE- and TM-polarized incident waves with close frequencies (Fig. 6). This demonstrates the beneficial effect of cross-polarization coupling induced by strips. For cloaking of a dielectric nanowire by helical graphene strips the frequency bandwidth, as opposed to minimal scattering efficiency, is highly sensitive to polarization of incident wave. This can be seen from Fig. 6. As this figure suggests, for optimal strip parameters the cloaking frequency has the widest bandwidth for TE-polarized waves and the narrowest one for TM-polarized waves.

For $\theta = 50°$ and variable values of f_r and u the scattering efficiency is depicted in Fig. 5(b). As is seen from this figure [compare also Figs. 3 and 6(b)], electromagnetic cloaking of a dielectric nanowire by helical graphene strips can be more efficient as compared to cloaking by a graphene monolayer, which is known to have a very high performance [15]. Note that in Eq. (5) there is no continuous transition from a graphene-coated nanowire to a bare dielectric cylinder as the strip width w (and u) approaches zero. In the extreme case of thin strips, one comes to a unidirectional conductor, which is conducting ($Z_\parallel$ is finite and approaches zero as $p \to 0$) in the direction parallel to the strips and perfectly insulating ($Z_\perp \to \infty$) in the perpendicular direction. The scattering problem for a dielectric cylinder coated by such helical strips made of a perfect electric conductor has been studied extensively in Refs. [31,32,39].

As Fig. 5 suggests, at the given angle of incidence α we can use parameters of graphene strips to tune the minimum visibility of the dielectric nanowire and thus to achieve the most efficient scattering suppression at a desired frequency for some u and θ. By proceeding similarly for different α we obtain the optimal values of u, θ and frequency, which correspond to the lowest averaged scattering for all incidence angles. For $u = 0.9$ ($\theta = 41°$), $u = 0.6$ ($\theta = 50°$), and $u = 0.3$ ($\theta = 54°$) the scattering efficiency Q_{sca} as a function of frequency f_r and incidence angle α of an illuminating dual-polarized wave is depicted in Fig. 7 and shows the best performance for all-angle cloaking of the dielectric nanowire at frequencies about 10.65, 12.35, and 16.4 THz, respectively. As u decreases, the cloaking ability of helical graphene strips is somewhat degraded. Despite this, in the frequency range of interest such strips suppress scattering from nanowire more efficiently as compared to graphene monolayer [see Fig. 4(a)]. The wide tuning band of the cloak in the form of helical graphene strips can also be seen from Fig. 8(a), which shows the optimal parameters of the strips versus design frequency f_r of dual-polarized all-angle cloaking. The corresponding values of Q_{sca}^{max} are shown in Fig. 8(b). One can see that the cloaking performance of helical graphene strips is rather high ($Q_{sca}^{max} < 5 \times 10^{-3}$) in a wide frequency band between 10 and 24 THz. In this band the value of $Q_{sca}^{max} = \max\{Q_{sca}(\alpha)\}$ was found to be attained for $\alpha = 0°$ (normal incidence). In the case of $\alpha = 0°$, Fig. 8(b) shows the relative bandwidth of frequencies, which satisfy the condition $Q_{sca} < 5 \times 10^{-3}$. From this figure one can notice that the frequency bandwidth of dual-polarized

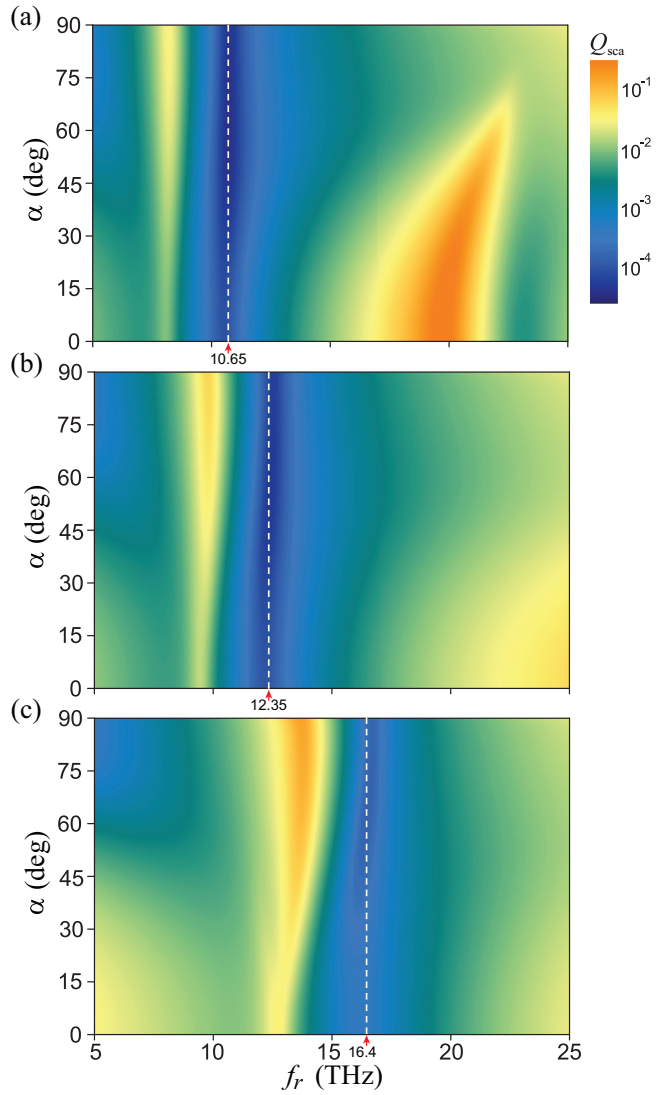

FIG. 7. Dual-polarized all-angle cloaking of a dielectric nanowire by helical graphene strips at frequencies (a) 10.65 THz ($u = 0.9, \theta = 41^\circ, Q_{sca}^{max} = 1.8 \times 10^{-4}$), (b) 12.35 THz ($u = 0.6$, $\theta = 50^\circ, Q_{sca}^{max} = 2 \times 10^{-4}$), and (c) 16.4 THz ($u = 0.3, \theta = 54^\circ, Q_{sca}^{max} = 8.1 \times 10^{-4}$).

cloaking of the dielectric nanowire by helical graphene strips is rather wide for design frequencies between 10 and 24 THz and reaches a maximum of 45% for $f_r = 11.25$ THz.

In addition, the improved ability of helical graphene strips to suppress scattering of dual-polarized waves from dielectric nanowire at any incidence angle can be demonstrated by inspection of the near-field distribution for the amplitude $|\mathbf{E}|$ of the total electric field. As desired cloaking frequency, we select 13.15 THz, which corresponds to the best performance of all-angle cloaking by graphene monolayer [see Fig. 4(a)]. This performance is then compared with that for helical graphene strips with optimal parameters $u = 0.51$ and $\theta = 51^\circ$ (see Fig. 8). In our simulations, the amplitude of electric field is normalized to the averaged value $(2\pi)^{-1} \int_0^{2\pi} d\varphi |\mathbf{E}^i|$ of the amplitude of incident wave at $r = 2.5R$. Therefore, the closer the normalized amplitude of the total electric field

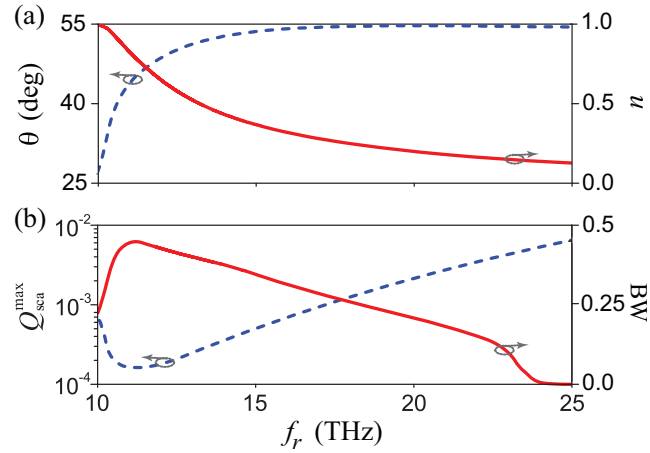

FIG. 8. (a) Optimal width-to-period ratio u and pitch angle θ of helical graphene strips versus design frequency of dual-polarized all-angle cloaking of a dielectric nanowire, and (b) corresponding value of Q_{sca}^{max}, which is achieved for normal wave incidence ($\alpha = 0^\circ$), together with the relative bandwidth (BW) of frequencies satisfying the condition $Q_{sca} < 5 \times 10^{-3}$ for $\alpha = 0^\circ$.

outside the nanowire to unity, the more efficient the scattering cancellation by the cloak. The near-field distribution of this amplitude for nanowires coated by graphene monolayer and helical graphene strips is shown in Fig. 9. From this figure one can clearly see that helical graphene strips indeed possess an improved ability for dual-polarized all-angle cloaking of the dielectric nanowire, in agreement with simulated results for scattering efficiency.

To show the robustness of all-angle cloaking by helical graphene strips to any polarization of incident wave we plot the scattering efficiency of a dielectric nanowire as a function of the full Poincaré sphere (Fig. 10). The axes of the Poincaré sphere are labeled in terms of the Stokes parameters. Linearly polarized states are arranged along the equator of the sphere,

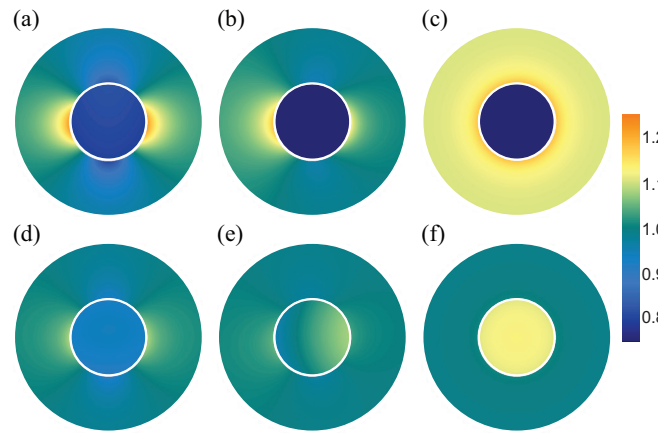

FIG. 9. Near-field distribution of amplitude of total electric field for a dielectric nanowire coated by graphene monolayer at (a) $\alpha = 0^\circ$, (b) $\alpha = 45^\circ$, and (c) $\alpha = 90^\circ$ and helical graphene strips ($u = 0.51$, $\theta = 51^\circ$) at (d) $\alpha = 0^\circ$, (e) $\alpha = 45^\circ$, and (f) $\alpha = 90^\circ$. The nanowire is illuminated by a dual-polarized wave with a frequency of 13.15 THz. The surface of the nanowire is depicted by the white line.

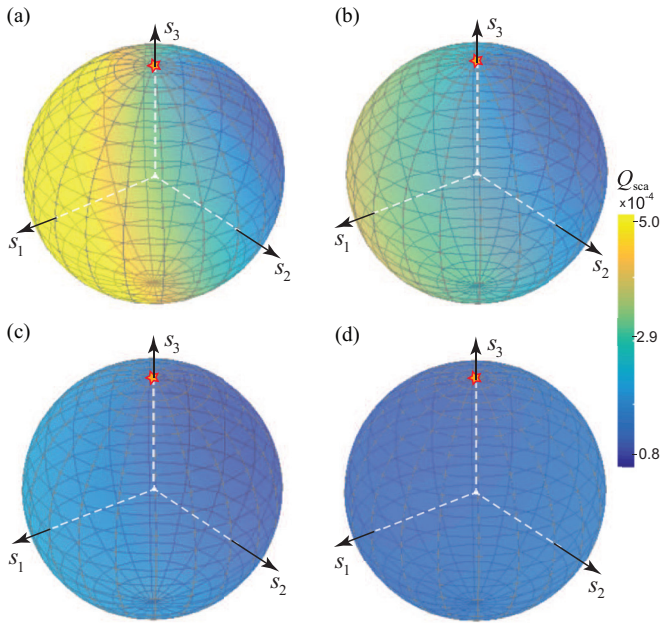

FIG. 10. Scattering efficiency of a dielectric nanowire coated by helical graphene strips ($u = 0.6$, $\theta = 50°$), which is mapped on the surface of a Poincaré sphere related to the polarization states of the incident wave with the frequency of 12.35 THz and angle of incidence (a) $\alpha = 0°$, (b) $\alpha = 30°$, (c) $\alpha = 45°$, and (d) $\alpha = 90°$. The star depicts a right circularly polarized wave with $Q = 0$, $\beta = 0$ ($P = 1$).

while right and left circularly polarized waves are located at its north and south poles, respectively. All other points of the sphere depict elliptically polarized states of the incident wave [40,41]. The design frequency is selected to be 12.35 THz. For this frequency we use the optimal parameters $u = 0.6$ and $\theta = 50°$ of helical graphene strips (Fig. 8). Although these parameters are found above for a circularly polarized wave, the scattering efficiency of the dielectric nanowire is seen to be small ($Q_{sca} < 5 \times 10^{-4}$) for any wave polarization and angle of incidence (Fig. 10). This demonstrates the high performance of all-angle cloaking of a dielectric nanowire by helical graphene strips, regardless of the polarization state of the incident wave.

Finally, we should note that in actual experimental conditions the cloaking performance of helical graphene strips can be deteriorated due to the finite length of a cylindrical object, which can have additional resonances in the scattering spectrum. However, as was demonstrated theoretically in Ref. [23] for plasmonic cloaking, such performance is moderately affected by truncation of the cylinder, even though the length of the cylinder only twice exceeds its diameter. Lately, for finite-length cylinders experimental realization of efficient mantle cloaking by a metasurface has been performed in Ref. [37].

V. CONCLUSIONS

Helical graphene strips have been proposed as a dual-polarized all-angle cloak for a dielectric nanowire. In the long-wavelength approximation, such strips have been treated as a graphene-based metasurface with averaged conductivity of tensor form. Their cloaking performance in the terahertz band has been found to be better than that of graphene monolayer, even though the normally incident dual-polarized wave is considered. This is because helical graphene strips coiled around nanowire can efficiently suppress scattering of both TE- and TM-polarized incident waves at single frequency due to cross-polarization coupling. It has been shown that this frequency can be widely tuned with pitch angle, period, and width of graphene strips. Moreover, these parameters of the strips can be further optimized to ensure all-angle cloaking of dielectric nanowire at a desired frequency for any polarization of incident wave. Such a property of helical graphene strips distinguishes them from other graphene-based metasurfaces used to cloak cylindrical objects in the terahertz band and makes them particularly attractive for a number of applications, including noninvasive sensing and low-interference communication.

ACKNOWLEDGMENT

This work was supported by Jilin University.

APPENDIX A: AVERAGED BOUNDARY CONDITIONS

Following the approach of Ref. [27], we derive here averaged boundary conditions at the surface of a dielectric cylinder coated by helical conducting strips.

Consider a metasurface in the form of two-dimensional conducting strips placed periodically at the interface between a dielectric cylinder of radius R and outside ambient with relative constitutive parameters ε_1, μ_1 and ε_2, μ_2, respectively. The strips have the period p and the width $w = up$. Let $\mathbf{i}_z$ and $\mathbf{i}_\varphi$ be the axial and the azimuthal unit vectors rotated by the angle θ with respect to the orthogonal vectors $\mathbf{i}_\parallel$ and $\mathbf{i}_\perp$, which are parallel and perpendicular to the strips, respectively.

Consider an electromagnetic wave propagated inside both media. The wave field has the following form: $\{\mathbf{E}, \mathbf{H}\} = \sum_{n=-\infty}^{\infty}\{\mathbf{E}^n, \mathbf{H}^n\}F_n$, where $F_n = \exp(-i\omega t + ik_z z + in\varphi)$. Assume that the wavelength $\lambda = 2\pi\omega/c$ of the electromagnetic wave far exceeds the period p of strips. In this case, there is a negligible contribution of the higher Bloch harmonics to the wave field at the metasurface area, where the averaged boundary conditions can be applied. For a dielectric cylinder coated by perfectly conducting strips, these conditions have the following form [42]:

$$\begin{aligned} E_{\parallel 1} &= E_{\parallel 2}, \quad E_{\perp 1} = E_{\perp 2}, \\ E_{\parallel 1} &= -iqZ_0 N\mu_\alpha \ln[\sin^{-1}(0.5\pi u)](H_{\perp 2} - H_{\perp 1}), \\ H_{\parallel 2} - H_{\parallel 1} &= iqZ_0^{-1} N\varepsilon_\alpha \ln\{\sin^{-1}[0.5\pi(1-u)]\}E_{\perp 1}, \end{aligned} \quad \text{(A1)}$$

where $q = 1 - k_\parallel^2/(\varepsilon_\alpha\mu_\alpha k^2)$, $N = 2p/\lambda$, $\varepsilon_\alpha = \varepsilon_1 + \varepsilon_2$, $\mu_\alpha = \mu_1\mu_2/(\mu_1 + \mu_2)$, $Z_0 = \sqrt{\mu_0/\varepsilon_0}$ is the impedance of free space, $k_\parallel^2 = \partial^2/\partial x_\parallel^2$ is the operator, $\partial/\partial x_\parallel = \sin\theta\,\partial/\partial z + \cos\theta R^{-1}\partial/\partial\varphi$, and $x_\parallel$ is the coordinate along the strips.

Averaged boundary conditions (A1) can be extended to the metasurface made of graphene strips with the finite conductivity $\sigma = \sigma(\omega)$. For this purpose, we introduce the graphene surface impedance $Z_g^{av} = u\sigma^{-1}$ averaged over the metasurface area. Using this impedance, we can rewrite the boundary

conditions (A1) at $r = R$ as

$$E^n_{\parallel 1} = E^n_{\parallel 2}, \quad H^n_{\parallel 2} - H^n_{\parallel 1} = -\sigma_\perp E^n_{\perp 1},$$
$$E^n_{\perp 1} = E^n_{\perp 2}, \quad H^n_{\perp 2} - H^n_{\perp 1} = \sigma_\parallel E^n_{\parallel 1}, \tag{A2}$$

where $\sigma_{\perp,\parallel} = (Z_{\perp,\parallel} + Z_g^{av})^{-1}$ are the principal components of the metasurface conductivity tensor

$$\hat{\boldsymbol{\sigma}} = \begin{pmatrix} \sigma_\perp & 0 \\ 0 & \sigma_\parallel \end{pmatrix}. \tag{A3}$$

Here $Z_\parallel = -iqZ_0 N\mu_\alpha \ln[\sin^{-1}(0.5\pi u)]$, $Z_\perp = iZ_0(qN\varepsilon_\alpha \ln\{\sin^{-1}[0.5\pi(1-u)]\})^{-1}$, and $k_\parallel^2 = (k_z \sin\theta + nR^{-1}\cos\theta)^2$.

In the cylindrical coordinates $\{r, \varphi, z\}$, the conductivity tensor (A3) is nodiagonal and the boundary conditions (A2) take the form (4).

The averaged boundary conditions (4) are accurate to at least first order in p/λ [43] and are valid for waves propagating in an arbitrary direction with respect to the strips. As u approaches unity, both $Z_\parallel$ and $Z_\perp$ vanish and the wire coating transforms to graphene monolayer [15–18]. The opposite extreme case is $u \to 0$. In this case, $Z_\perp$ tends to infinity and one obtains the boundary conditions for the unidirectional conductor [31,32,39]. The boundary conditions (4) reduce to those for a dielectric cylinder coated by axial and azimuthal conducting strips for $\theta = 0^\circ$ and $\theta = 90^\circ$ [25,33], respectively.

APPENDIX B: HARMONIC AMPLITUDES

The substitution of (1)–(3) into boundary conditions (4) leads to the following system of linear algebraic equations for unknown amplitudes of harmonic with azimuthal index n:

$$B_n - D_n = -iPJ_n(k_2R), \tag{B1}$$

$$A_n\lambda_1\frac{k_2}{k_1} + iB_n\frac{nk_zk_2}{kR}\left(\frac{1}{k_2^2} - \frac{1}{k_1^2}\right) - C_n\lambda_2 = J_n'(k_2R), \tag{B2}$$

$$A_n\left(1 + i\sigma_{\varphi\varphi}\frac{k}{k_1}\lambda_1\right) + B_n\left(\sigma_{\varphi\varphi}\frac{nk_z}{k_1^2R} - \sigma_{\varphi z}\right) - C_n = J_n(k_2R), \tag{B3}$$

$$A_n\left(\frac{nk_z}{k_1^2R} + \frac{ik}{k_1}\sigma_{z\varphi}\lambda_1\right) - B_n\left(\frac{i\varepsilon_1 k}{k_1}\lambda_1 + \sigma_{zz} - \sigma_{z\varphi}\frac{nk_z}{k_1^2R}\right)$$
$$- C_n\frac{nk_z}{k_2^2R} + iD_n\frac{\varepsilon_2 k}{k_2}\lambda_2 = \frac{nk_z}{k_2^2R}J_n(k_2R) - \frac{\varepsilon_2 k}{k_2}PJ_n'(k_2R), \tag{B4}$$

where $A_n = a_nJ_n(k_1R)$, $B_n = b_nJ_n(k_1R)$, $C_n = c_nH_n^{(1)}(k_2R)$, $D_n = d_nH_n^{(1)}(k_2R)$, $\lambda_1 = J_n'(k_1R)/J_n(k_1R)$, $\lambda_2 = H_n'^{(1)}(k_2R)/H_n^{(1)}(k_2R)$, and a_n, b_n, c_n, and d_n are the amplitudes of azimuthal (Mie) harmonic.

APPENDIX C: GRAPHENE DESCRIPTION

Ignoring the quantum finite-size effect of graphene [44], the nanowire coating is treated as an infinitely thin graphene monolayer having the macroscopic surface conductivity σ, which depends on the angular frequency $\omega = 2\pi f_r$, the chemical potential μ_c, the ambient temperature T, and the scattering rate of charge carriers $\Gamma = 1/\tau$. The surface conductivity of graphene consists of intraband and interband components $\sigma = \sigma_{\text{intra}} + \sigma_{\text{inter}}$, which are described by the Kubo formalism [34]:

$$\sigma_{\text{intra}} = \frac{2ie^2k_BT}{\hbar^2\pi(\omega + i\Gamma)}\ln\left[2\cosh\left(\frac{\mu_c}{2k_BT}\right)\right],$$
$$\sigma_{\text{inter}} = \frac{e^2}{4\hbar\pi}\left[\frac{\pi}{2} + \arctan\left(\frac{\hbar\omega - 2\mu_c}{2k_BT}\right)\right.$$
$$\left. - \frac{i}{2}\ln\frac{(\hbar\omega + 2\mu_c)^2}{(\hbar\omega - 2\mu_c)^2 + (2k_BT)^2}\right]. \tag{C1}$$

Here k_B is the Boltzmann constant, $\hbar$ is the reduced Planck constant, and e is the electron charge. The chemical potential μ_c is related to the carrier density N_c as $\mu_c = \hbar v_F\sqrt{\pi N_c}$, where $v_F \simeq 10^6$ m/s is the Fermi velocity of electrons in graphene.

[1] R. Fleury, F. Monticone, and A. Alù, Invisibility and Cloaking: Origins, Present, and Future Perspectives, Phys. Rev. Appl. **4**, 037001 (2015).

[2] S. A. Cummer, B.-I. Popa, D. Schurig, D. R. Smith, and J. Pendry, Full-wave simulations of electromagnetic cloaking structures, Phys. Rev. E **74**, 036621 (2006).

[3] Z. Ruan, M. Yan, C. W. Neff, and M. Qiu, Ideal Cylindrical Cloak: Perfect but Sensitive to Tiny Perturbations, Phys. Rev. Lett. **99**, 113903 (2007).

[4] H. Chen, B.-I. Wu, B. Zhang, and J. A. Kong, Electromagnetic Wave Interactions with a Metamaterial Cloak, Phys. Rev. Lett. **99**, 063903 (2007).

[5] B. Zhang, H. Chen, B.-I. Wu, Y. Luo, L. Ran, and J. A. Kong, Response of a cylindrical invisibility cloak to electromagnetic waves, Phys. Rev. B **76**, 121101(R) (2007).

[6] A. Alù and N. Engheta, Achieving transparency with plasmonic and metamaterial coatings, Phys. Rev. E **72**, 016623 (2005).

[7] A. Alù and N. Engheta, Multifrequency Optical Invisibility Cloak with Layered Plasmonic Shells, Phys. Rev. Lett. **100**, 113901 (2008).

[8] M. G. Silveirinha, A. Alù, and N. Engheta, Cloaking mechanism with antiphase plasmonic satellites, Phys. Rev. B **78**, 205109 (2008).

[9] M. G. Silveirinha, A. Alù, and N. Engheta, Infrared and optical invisibility cloak with plasmonic implants based on scattering cancellation, Phys. Rev. B **78**, 075107 (2008).

[10] S. Tricarico, F. Bilotti, A. Alù, and L. Vegni, Plasmonic cloaking for irregular objects with anisotropic scattering properties, Phys. Rev. E **81**, 026602 (2010).

[11] A. Alù, Mantle cloak: Invisibility induced by a surface, Phys. Rev. B **80**, 245115 (2009).

[12] P.-Y. Chen and A. Alù, Mantle cloaking using thin patterned metasurfaces, Phys. Rev. B **84**, 205110 (2011).

[13] A. Alù and N. Engheta, Cloaking a receiving antenna or a sensor with plasmonic metamaterials, Metamaterials **4**, 153 (2010).

[14] S. Vellucci, A. Monti, M. Barbuto, A. Toscano, and F. Bilotti, Satellite applications of electromagnetic cloaking, IEEE Trans. Antennas Propag. **65**, 4931 (2017).

[15] P.-Y. Chen and A. Alù, Atomically thin surface cloak using graphene monolayers, ACS Nano **5**, 5855 (2011).

[16] M. Riso, M. Cuevas, and R. A. Depine, Tunable plasmonic enhancement of light scattering and absorption in graphene-coated subwavelength wires, J. Opt. **17**, 075001 (2015).

[17] M. Naserpour, C. J. Zapata-Rodríguez, S. M. Vuković, H. Pashaeiadl, and M. R. Belić, Tunable invisibility cloaking by using isolated graphene-coated nanowires and dimers, Sci. Rep. **7**, 12186 (2017).

[18] V. I. Fesenko, V. I. Shcherbinin, and V. R. Tuz, Multiple invisibility regions induced by symmetry breaking in a trimer of subwavelength graphene-coated nanowires, J. Opt. Soc. Am. A **35**, 1760 (2018).

[19] P.-Y. Chen, J. Soric, Y. R. Padooru, H. M. Bernety, A. B. Yakovlev, and A. Alù, Nanostructured graphene metasurface for tunable terahertz cloaking, New J. Phys. **15**, 123029 (2013).

[20] H. M. Bernety and A. B. Yakovlev, Cloaking of single and multiple elliptical cylinders and strips with confocal elliptical nanostructured graphene metasurface, J. Phys.: Condens. Matter **27**, 185304 (2015).

[21] A. Forouzmand and A. B. Yakovlev, Electromagnetic cloaking of a finite conducting wedge with a nanostructured graphene metasurface, IEEE Trans. Antennas Propag. **63**, 2191 (2015).

[22] M. Danaeifar and N. Granpayeh, Wideband invisibility by using inhomogeneous metasurfaces of graphene nanodisks in the infrared regime, J. Opt. Soc. Am. B **33**, 1764 (2016).

[23] A. Alù, D. Rainwater, and A. Kerkhoff, Plasmonic cloaking of cylinders: Finite length, oblique illumination and cross-polarization coupling, New J. Phys. **12**, 103028 (2010).

[24] A. Monti, J. C. Soric, A. Alù, A. Toscano, and F. Bilotti, Anisotropic mantle cloaks for TM and TE scattering reduction, IEEE Trans. Antennas Propag. **63**, 1775 (2015).

[25] Y. R. Padooru, A. B. Yakovlev, P.-Y. Chen, and A. Alù, Analytical modeling of conformal mantle cloaks for cylindrical objects using sub-wavelength printed and slotted arrays, J. Appl. Phys. **112**, 034907 (2012).

[26] F. Monticone and A. Alù, Invisibility exposed: Physical bounds on passive cloaking, Optica **3**, 718 (2016).

[27] V. I. Shcherbinin, V. I. Fesenko, and V. R. Tuz, Low-loss forward and backward surface plasmons in a semiconductor nanowire coated by helical graphene strips, J. Opt. Soc. Am. B **35**, 2066 (2018).

[28] W. Xu and T.-W. Lee, Recent progress in fabrication techniques of graphene nanoribbons, Mater. Horiz. **3**, 186 (2016).

[29] C. F. Bohren and D. R. Huffmann, *Absorption and Scattering of Light by Small Particles* (Wiley-Interscience, New York, 2010).

[30] J. R. Wait, Scattering of a plane wave from a circular dielectric cylinder at oblique incidence, Can. J. Phys. **33**, 189 (1955).

[31] A. A. Kishk and P.-S. Kildal, Asymptotic boundary conditions for strip-loaded scatterers applied to circular dielectric cylinders under oblique incidence, IEEE Trans. Antennas Propag. **45**, 51 (1997).

[32] L. K. Hady and A. A. Kishk, Electromagnetic scattering from conducting circular cylinder coated by meta-materials and loaded with helical strips under oblique incidence, Prog. Electromagn. Res. B **3**, 189 (2008).

[33] Z. Sipus, M. Bosiljevac, and A. Grbic, Modelling cascaded cylindrical metasurfaces using sheet impedances and a transmission matrix formulation, IET Microw. Antennas Propag. **12**, 1041 (2018).

[34] L. A. Falkovsky and S. S. Pershoguba, Optical far-infrared properties of a graphene monolayer and multilayer, Phys. Rev. B **76**, 153410 (2007).

[35] P. Yu, V. I. Fesenko, and V. R. Tuz, Dispersion features of complex waves in a graphene-coated semiconductor nanowire, Nanophotonics **7**, 925 (2018).

[36] H. Yan, T. Low, W. Zhu, Y. Wu, M. Freitag, X. Li, F. Guinea, P. Avouris, and F. Xia, Damping pathways of mid-infrared plasmons in graphene nanostructures, Nat. Photonics **7**, 394 (2013).

[37] J. C. Soric, P. Y. Chen, A. Kerkhoff, D. Rainwater, K. Melin, and A. Alù, Demonstration of an ultralow profile cloak for scattering suppression of a finite-length rod in free space, New J. Phys. **15**, 033037 (2013).

[38] T. J. Arruda, R. Bachelard, J. Weiner, and P. W. Courteille, Tunable Fano resonances in the decay rates of a pointlike emitter near a graphene-coated nanowire, Phys. Rev. B **98**, 245419 (2018).

[39] P. Chen, F. Monticone, and A. Alù, Suppressing the electromagnetic scattering with an helical mantle cloak, IEEE Antennas Wireless Propag. Lett. **10**, 1598 (2011).

[40] H. G. Jerrard, Transmission of light through birefringent and optically active media: The Poincaré sphere, J. Opt. Soc. Am. **44**, 634 (1954).

[41] E. Collett and B. Schaefer, Visualization and calculation of polarized light. I. The polarization ellipse, the Poincaré sphere and the hybrid polarization sphere, Appl. Opt. **47**, 4009 (2008).

[42] S. Ye. Bankov and I. V. Levchenko, Equivalent boundary conditions for a closely spaced ribbon grating at the interface of two media, Sov. J. Commun. Technol. Electron. **34**, 67 (1989).

[43] S. Tretyakov, *Analytical Modeling in Applied Electromagnetics* (Artech House, Boston, 2003).

[44] S. Thongrattanasiri, A. Manjavacas, and F. J. García de Abajo, Quantum finite-size effects in graphene plasmons, ACS Nano **6**, 1766 (2012).